Direct Evidence of Salinity Difference Effect on Water Transport in Oil

Pore-Scale Mechanisms

Yan, Lifei; Golestan, Mohammad Hossein; Zhou, Wenyu; Hassanizadeh, S. Majid; Berg, Carl Fredrik; Raoof, Amir

Important note
To cite this publication, please use the final published version (if applicable).
Please check the document version above.

Direct Evidence of Salinity Difference Effect on Water Transport in Oil: Pore−Scale Mechanisms

Lifei Yan,* Mohammad Hossein Golestan, Wenyu Zhou, S. Majid Hassanizadeh, Carl Fredrik Berg, and Amir Raoof*
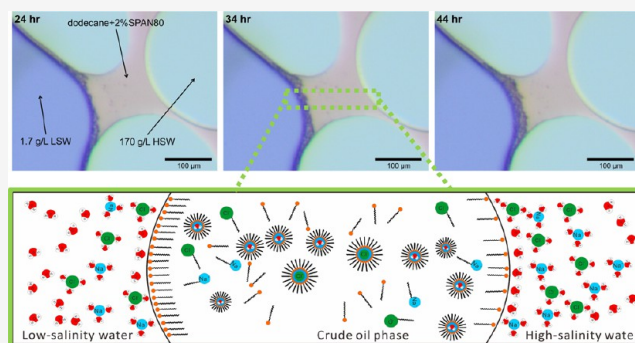
ACCESS | Metrics & More | Article Recommendations | Supporting Information

ABSTRACT: Low salinity water flooding is a common technique for enhancing oil recovery; however, the mechanism behind the low-salinity effect, positive or negative, is still not fully understood. In the proposed mechanisms, osmosis and emulsification are considered as two potential reasons for explaining the oil remobilization, but the specific contributions on the remobilization are not well studied at pore-scale. In this article, we performed a series of microfluidic experiments to investigate the movement of constrained oil between invading low-salinity brine and residual high-salinity brine. We find that various salinity contrasts over oil films cause different water fluxes through the oil and swelling areas of the trapped brine, resulting in the relocation of oil phases within the pore spaces. A higher salinity contrast (1.7−170 g/L salt concentrations) provides a faster water penetration in oil phases. In the presence of an oil-soluble surfactant, spontaneous emulsification occurs at the interface of low-salinity brine/oil, which enhances almost 100 times the water flux in two oil phases (*n*-heptane and *n*-dodecane). We directly observe pore-scale spontaneous emulsification at the low-salinity brine/oil interface but not at the high-salinity brine/oil interface. Furthermore, two scenarios for explaining water transport through the oil phase are proposed: water diffusion due to chemical potential gradient and water transport via reverse micelle or microemulsions movement.

1. INTRODUCTION

1.1. Suggested Mechanisms of Low-Salinity Effect. It has been observed that a lower ionic strength in flooding brine gives higher oil recovery, commonly termed the low-salinity (LS) effect. Over the past 30 years, researchers have proposed around 13 different mechanisms for this low-salinity effect, including: fine mobilization,[1] wettability change of rock surface,[2] multiple ion exchange (MIE),[3] double layer expansion based on the theory of Derjaguin, Landau, Verwey, and Overbeek (DLVO),[4] interfacial tension and pH effect,[5,6] and microemulsion and osmosis effect.[7,8] However, no consensus has yet been reached on the relative importance of different mechanisms. The main mechanisms and their relationships are given in Figure 1. Four main potential mechanisms and their drawbacks are briefly discussed below.

1.1.1. Fine Migration. Systematic experimental work for low-salinity effects was done by Tang and Morrow[9] (1999). They conducted a series of core-flooding experiments and proposed that injecting low salinity water into clay-rich cores potentially mobiles fine clay particles and partial detachment of mixed-wet fines from solid surfaces. Fine migration leads to a partial mobilization of residual oil, which attaches fine particles. Alhuraishawy et al.[10] studied two key factors, salinity value and oil aging time, by performing core-flood experiments for
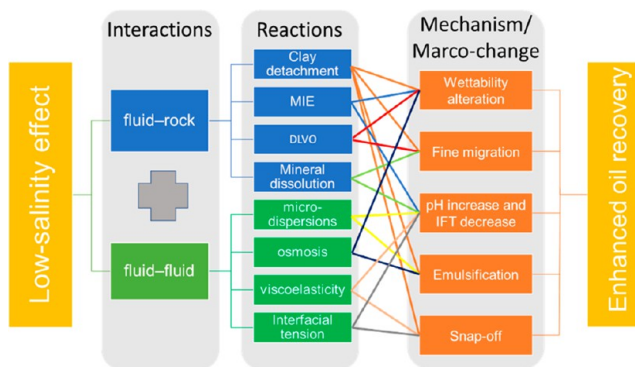

Figure 1. Suggested mechanisms for low-salinity effects and their relations.

imbibition and imaging experiments with scanning electron microscopy (SEM). They came to a similar conclusion that low water salinity injection induces mineral dissolution and sand migration which redistributes the flow pathways and increases oil displacement and sweep efficiency. Although several experimental observations have been used to support this mechanism, contradictory results have grown in number, as well. Lager, Webb, Black, Singleton, and Sorbie[3] reported numerous low-salinity core-flooding experiments with additional oil recovery but did not observe fine mobilization or obvious permeability reductions in the reservoir conditions.

1.1.2. Wettability Alteration. Jadhunandan and Morrow[11] pointed that the saturation of initial water determines the rock wettability. Given a higher initial water saturation, the rock surface renders water-wet. Low-salinity effect possibly relates to wettability change of the rock surface which alters the solid surface to stronger water-wet, which can improve oil recovery. Sharma and Filoco[12] proved that the core which performed an improved oil recovery had the wettability change from strongly water-wet close to middle wet, especially for the cores with lower ionic strength. Vledder et al.[13] acquired field observations of wettability change in rock surface from oil-wet to water-wet in the Omar field in Syria after applying a LSW flooding that enhanced oil recovery. They collected the laboratory data from imbibition experiments in cores and a single well in an analogue field to support their observation. Although wettability alteration is considered as a main mechanism for explaining the low ionic strength effect, the wettability alteration itself can be caused by multiple factors, such as DLE, MIE, mineral dissolution, etc.

1.1.3. Double Layer Expansion and MIE. The Derjaguin−Landau−Verwey−Overbeek (DLVO) theory is applied to correlate the electrokinetic of solid surface to the thermodynamic interaction related to the wettability alteration and the thin liquid film.[14] The total disjoining pressure can be described by the amount of van der Waals forces (vdW), structural forces, and electrostatic double layer (EDL). Ding and Rahman[15] proposed oil adsorption on the carbonate substrate was caused by the opposite charge polarity on the rock/brine/oil interfaces and explained the low-salinity effect on the force balance at the interfaces with using the DLVO theory. Low ionic strength leads to a reduced attractive force between the rock/brine/oil interfaces and an increased Debye length, which results in double layer expansion. The expansion enhances the growth of water film and alters rock from oil-wet to water-wet.[16,17] Recently, Aseyednezhad et al.[18] derived a 1-dimensional Nernst−Planck−Poisson model, and analyzed the dynamic pressure field evolution within an expanding brine film under the influence of ionic strength gradient. Ion exchange and geochemical reactions are considered to be potential factors for changing the wettability of rock-brine systems.

Multivalent ionic exchange is a mechanism of ion exchanges between the brine/oil interface and brine/rock interface, resulting in the desorption of oil molecule or droplets from the solid surface.[19] Lager, Webb, Black, Singleton, and Sorbie[3] proposed the mechanism for describing cation exchange, ligand bonding, and cation and water bridging on a sandstone surface. They believed that low-salinity water flooding induces a stronger ligand bonding than the other two factors. Therefore, carboxylic acids prefer to detach from the solid surface. Other researchers gave a similar mechanism for chalk formations and carbonate reservoirs.[20,21]

However, the MIE mechanism is widely studied for chalk or pure calcite.[22] Moreover, some works are showing contradictory results of no ion exchange reactions during LSWF. Tetteh et al.[23] conducted core flooding experiments using various types of salinity brines. They monitored the ionic composition of the effluent brine and pointed out that no obvious ion exchange appeared in the tertiary mode of flooding with or without low salinity brines. The coexistence of DLE and MIE might contribute to the wettability changes in some extent, but which one impacts more is still unclear. Additionally, both theories lack direct and solid evidence to support the explanations, although some macroobservations show water film generation and wettability alteration.

1.1.4. pH Increase and IFT Decrease. McGuire, Chatham, Paskvan, Sommer, and Carini[6] proposed that a low salinity environment can increase pH and decrease IFT, resulting in a wettability alteration. Increased pH is induced by hydrogen ion exchange between water and adsorbed sodium ions. The increase imposes a significant change of zeta potential on the rock and helps organic material desorption from the clay surfaces.[24] Zhang et al.[25] reported a slight rise in pH after LS brine injection. Decreased IFT is related to the salinity and natural surface-active agents in the crude oil forming water/oil or oil/water emulsions, which may improve the surface elasticity and prevent snap-off at the oil/brine interface.[26] Mokhtari et al.[27] noticed that IFT reached the lowest value when crude oil contacted brine in a core for 48 h, and further observed a decrease pH in effluent and EOR. However, mechanisms between increased pH and decreased IFT do not have a corresponding relationship. Sheng[28] reviewed the pH change before and after low-salinity brine injection in literature and mentioned that some cases did not have a pH change. He pointed out that the pH in liquid acquired from the field was smaller than the value of emulsification and needs to be confirmed for the low-salinity brine flooding.

During the low-salinity brine injection, the interactions among crude oil, brine, and rock may be categorized into two major interactions: fluid−rock and fluid−fluid interactions. Because of the complicated system of brine/rock/crude oil, many mechanisms may be active and interacting. Hong et al.[29] described the various chemical components, e.g., alkalis, surfactants and polymers, play important roles in the interface phenomena of liquid−liquid, gas−liquid, and gas−solid interfaces, which leads to the multiphase fluid flow characteristics and the changes in adsorption behavior of phases. For instance, fine migration is related to the detachment of clay particles and the mineral dissolution. Due to the mineral dissolution, low-salinity solution gains a bigger viscosity. In the theory of MIE, divalent cations that attaches on the solid surface are replaced by hydrogen ions, which increases local pH in the solution[24] and improves the fines release.[30] Besides, the increased pH induces the IFT reduction and water−oil emulsification.[31] Low-salinity effect is therefore expected to be caused by multiple mechanisms which involve complex properties of porous media.

1.2. Osmosis Effects in LSWF. The mechanisms for liquid−liquid interactions including osmosis, reduced interfacial tension, and emulsification are commonly overlooked in the efficiency of the oil recovery by mobilizing stagnant oil and changing the system wettability.[32] The number of publications every year related to the topics of osmosis and emulsification as low salinity effects is displayed in Figure 2. After 2010, the number of studies on each topic increased rapidly. Never-
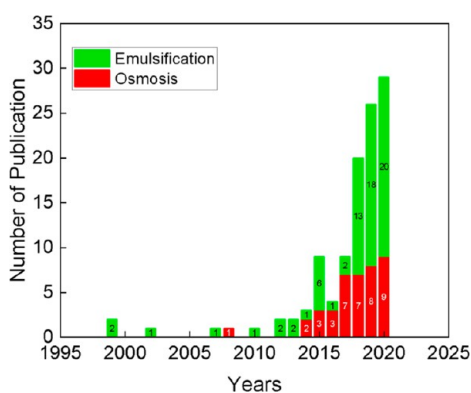
Figure 2. Number of publications from the 1990s to 2020 related to the low salinity effects of osmosis and emulsification.

theless, few researchers have taken both effects into account to explain the enhanced oil recovery from low salinity.

Osmosis is a physical process as a result of salinity contrast, accompanying an osmotic water flux through a selectively permeable membrane. Young and Low[33] conducted a laboratory experiment using a clay compacted cell and demonstrated that the movement of solution through layers of clay is related to salt concentration difference and the corresponding hydraulic pressure. Marine and Fritz[34] proposed an osmotic model to explain anomalous hydraulic heads in the Dunbarton Triassic basin, with consideration of clay as a nonideal membrane that includes some solute components. Neuzil[35] pointed out that the magnitude of anomalous hydraulic heads depends primarily upon the solute concentration differences across the membrane, and the membrane properties such as porosity, permeability and rock surface charges. Fakcharoenphol et al.[36] reported experimental and numerical modeling studies of osmotic pressure effect on oil recovery and conducted imbibition experiments using a laminated formation shale core to estimate the potential of low-salinity waterflooding in Bakken. They proved that chemical osmosis contributes to the withdrawal of crude oil from stagnant pores that low-salinity brine cannot directly reach. They compared the results from their mathematical model with the experimental data and indicated that osmotic pressure was the mechanism for enhancing countercurrent flow of oil in the core. Similarly, Takeda et al.[28] performed chemical osmosis experiments with clay-bearing reservoir rocks and relevant simulations.

Clay or micropores play as a semipermeable membrane that allows water molecules to penetrate, which consequently causes the pressure difference in the porous formation. Schmid et al.[37] extended the classical method of entry pressure for describing salinity-dependent capillary pressure and displacement events. The micropores with two throat diameters are filled with a nonwetting phase and a wetting phase comprising two residual brines. Osmotic flow changes the capillary entry pressure and induces pore-invasion phenomena, e.g., piston-like displacement and snap-off, depending on the local salt concentration. They concluded that the osmosis effect on multiphase flow in many cases is not distinguishable from a wetting change.

The mechanism of oil acting as a membrane for low-salinity water flooding was first proposed by Sandengen and Arntzen.[8] They observed the movement of oil droplets under the influence of an osmotic gradient in a 1 mm diameter glass tube.

Later, they performed a capillary experiment to directly show osmotic water transport through oil. Besides, quasi-2D microfluidic experiments for mimicking the tertiary mode of low-salinity water flooding were conducted as well by Sandengen et al.[38] They noticed the expansion of the connate high-salinity water due to the salinity gradient. Therefore, they concluded that the oil inside an oil-wet porous medium acts as a semipermeable membrane, which induces the relocation of residual oil and has the capability of yielding additional oil recovery. Yan et al.[39,40] have shown the osmotic effect on the oil remobilization from molecular to pore scale, based on various investigation tools including dynamic molecular simulation, microcapillary, and micromodel experiments. The results in the literature indicated that osmosis could increase oil migration and have a positive effect on oil recovery during low salinity water flooding. In this paper, we will consider the oil itself as a membrane for osmotic water transport.

1.3. Emulsification Effects in LSWF. In the study of microdispersion/emulsion, Emadi and Sohrabi[7] conducted the microfluidic experiments to capture the interactions and microemulsion generation around oil/water interfaces. Spontaneous emulsification is a chemical process of two immiscible liquids contacting each other and emulsion generated without any external thermal or mechanical energy source until the system of two liquids gains a minimum total free energy.[41] When the surfactant concentration is above a critical concentration, known as the critical micelle concentration (CMC), the surfactant molecules can assemble the insoluble phase molecules and create the micelles in the soluble phase. In nature, some polar components, such as naphthenic acids, resins and asphaltenes, have the potential to act as active emulsifiers contributing to emulsion formation.[42] Water in oil (W/O) and oil in water (O/W) emulsions, or more complicated emulsions, are usually found in the process of water or surfactant flooding.[43] When water meets with crude oil, the surface-active components would adsorb onto the oil–water interface and each sides groups can find the greatest affinity to make the total free energy reaching minimum, which leads the spontaneous formation of micelles at nano- to pore-scale.[44]

Wu and Firoozabadi[45] imaged the spontaneous emulsification close to the oil–aqueous phase interface and concluded that destabilization of water-in-oil emulsions in the bulk oil phase may improve the efficiency of oil displacement. Du et al.[46] reported a similar phenomenon in their microfluidic experiments and directly captured the dynamic process of water-in-oil emulsions formation that improved the oil sweep efficiency. Salehpour et al.[47] performed a series of microscale experiments to study the influence of fluid–fluid interactions on the fluid flow and oil recovery efficiency during low-salinity waterflooding. They directly captured the intensified spontaneous formation of W/O emulsions at the interface at a low flow rate and the accompanying pressure fluctuation induced by emulsion division and rupture. They, therefore, believed that emulsion formation leads to an additional contribution to enhanced oil recovery by LSWF.

Some studies have shown the relationship between the electrolyte concentration and emulsion size. Maaref and Ayatollahi[48] prepared the samples of w/o emulsions with different seawater samples from fields and measured the emulsion size and gave log-normal function of emulsion droplet size distribution, which showed that the low-salinity condition had more stable and uniform emulsions. Behera et
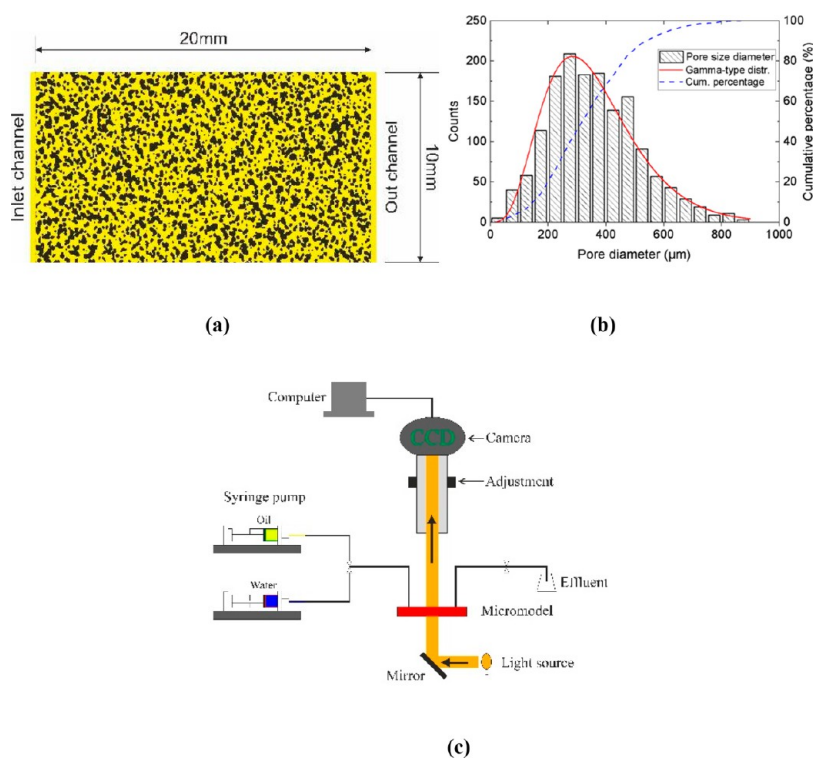
Figure 3. (a) Planar view of the microchip porous domain and schematic of micromodel setup. Solid grain is in black and pore space is in yellow. (b) Pore diameter distribution and a gamma-type fitted curve. (c) The experimental setup.

al.[49] studied the effects of surfactant, salt and oil concentrations on foaming in micellar solutions. They found that the initial foam volume generated in a blender test increased with an increasing surfactant concentration but decreased with an increasing salt concentration. Besides, the surface tension decreased with both of the increase in surfactant concentration and salt concentration.[50] However, the descriptions of the dynamic emulsification and its quantitative effect on water transport are not fully described yet. For instance, how the water behaves in the oil phase because of the salinity contrast is not quite clear. Thus, quantitative analysis of the osmosis effect is still necessary to explain the phenomenon. Moreover, the descriptions of dynamic emulsification and its effect on water transport are not fully described yet.

In this work, we attempt to answer two research questions: How to quantify the effect of salinity contrast on water transport in the oil phase, and what is the contribution of emulsification to water transport? Earlier, in experiments in a single glass capillary,[39] we have confirmed that the salinity differential caused the remobilization of a crude oil globule sandwiched between HSW and LSW regions. However, we could not clearly quantify the water transport in oil and emulsification influence due to the complexity of crude oil. Here, we describe a series of microfluidic experiments on a microfluidic device. We performed various experiments with three different salinity contrasts and four synthetic oils (two alkanes and two surfactant-added alkanes) to elucidate those two aspects in a relatively realistic pore-scale system. We sequentially inject high-salinity brine, oil, and low-salinity brine into a microchip to establish oil films sandwiched between disconnected high-salinity water and connected low-salinity water under no flow conditions. All phases are continuously observed more than 70 h under a high-resolution microscope. Through these experiments, we can monitor the oil movement

induced by the expansion of the trapped HSW area. We are further able to distinguish the effect of surfactants in the oil phase. Furthermore, the evaluation of salinity contrasts is described by an analytical method.

In our article, Section 2 describes the microfluidic experiments and the optic setup. Section 3 presents the experimental results and discusses the phenomenon of HSW expansion. We introduce a method for quantitatively analyzing water transport in the oil phase. Based on these results, the impacts of salinity and water-in-oil emulsification are discussed. The dynamic pore-scale emulsification is visualized and described as well. In Section 4, we provide two explanations for water transport through the oil phase: water diffusion in pure alkanes and microemulsions transport toward the HSW–oil interface.

2. MICROFLUIDIC EXPERIMENTS METHODOLOGY

2.1. Microchip Fabrication. We utilize a microscope connected to a 9 megapixel digital camera for providing a resolution of 1.21 pixel per micrometer. The microchip has a porous domain of 10 mm (width) × 20 mm (length). Permeability and porosity are 2.5 Darcy and 0.57, respectively. Note that the porosity and permeability are expected not to affect water transport through the oil phase in the pore space of microchips. The microchip is fabricated by borosilicate glass for gaining an inner porous structure (black areas in Figure 3) that is supposed to mimic the grain shapes of a sandstone core. The pore structure is fabricated through an acid etching method for reaching a uniform depth of 20 μm.

In order to prevent water films along the solid inner surface, we use a silanization solution of 1,7-Dichloro-1,1,3,3,5,5,7,7-octamethyltetrasiloxane to coat a hydrophobic surface inside the microchip. The details of silanization method can be found in our previous article.[40] The contact angles of water,
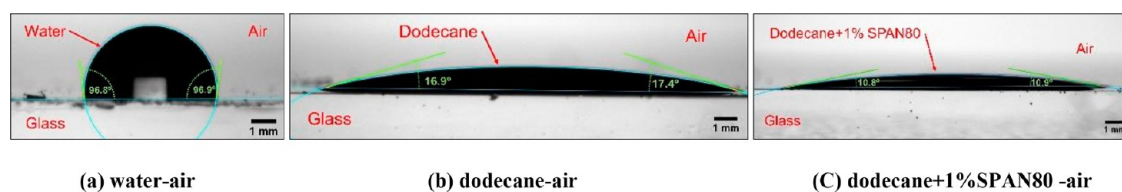
Figure 4. Measurements of contact angle after wettability treatment on glass microchips.

dodecane, and dodecane + SPAN80 droplets in air are ≈97°, ≈17°, and ≈10°, respectively, as shown in Figure 4.

2.2. Fluid Preparation and Formation of LSW–Oil–HSW Sequences in Microfluidics. Three types of salty water and four types of alkanes are prepared: the three brines are distinguished by their salt content of 1.7 g/L LSW, 50 g/L LSW, and 170 g/L HSW, and the four alkanes are pure dodecane, dodecane with SPAN 80, pure heptane, and heptane with SPAN 80. *n*-Heptane and *n*-dodecane are selected as the oil phases for verifying the effect of carbon chain lengths. The molecular chain characteristics and group bonding have influence on the water–oil emulsion structure and stability.[29] All oil liquids are equilibrated with high-salinity water for 24 h. To investigate the emulsification effect, we added hydrocarbon-soluble surfactant SPAN 80 to both dodecane and heptane for creating the water-in-oil microemulsions in the oil phase. Span80 is a nonionic and hydrocarbon-soluble surfactant, which helps to form water-in-oil emulsions in the hydrocarbon liquids. The concentration of 1% w/w SPAN 80 ($\approx 1.75 \times 10^{-2}$ mol/L) far exceeded the critical micelle concentration for heptane (1.8×10^{-5} mol/L) and dodecane (1.9×10^{-5} mol/L).[48] High-salinity water (170 g/L salt concentration) was made with deionized water and 4 different salts ($NaCl$, Na_2SO_4, $MgCl_2 \cdot 6H_2O$, and $CaCl_2 \cdot 2H_2O$) to mimic one type of formation brine. Then, we diluted the HSW to obtain two solutions with concentrations of 50 and 1.7 g/L LSW. The components of HSW are shown in Table 1. All experiments are conducted at room temperature.

Table 1. Components of HSW at Room Conditions

Ion type	Compound	Mol. weight (g/mol)	Concentration (mg/L)
Na^+	$NaCl$	58.44	50374
Ca^{2+}	$CaCl_2 \cdot 2H_2O$	146.8	10983
Mg^{2+}	$MgCl_2 \cdot 6H_2O$	203.1	1586
SO_4^{2+}	Na_2SO_4	142.04	234
Cl^-		109181	
TDS[a]			172358

[a]Total dissolved solids.

We dyed the low-salinity water with Methylene blue to make LSW appear to be blue under the microscope and oil with Sudan red to show brown in the acquired images. To generate the LSW–oil–HSW sequences with disconnected HSW and sandwiched oil inside a microchip, we perform the following procedure: first saturate chips with HSW, then inject the oil phase at a flow rate 100 μL/min; last, inject LSW with a flow rate 5 μL/min (which corresponds to a rate about 0.4 ft/day). The remaining HSW stays in some of the small and/or dead-end pores in the microchip. We wait another 30 min to allow the fluids inside the microchip to stabilize. Finally, we close the inlet and outlet valves to prevent external disturbance.

To calculate the capillary number during fluid injection, we assumed that the surface tension values for the oil phases

(heptane, dodecane, heptane+SPAN80, and dodecane + SPAN80) were within the range of 1−50 N/m.[49] The large range is due to the addition of the surfactant SPAN80, which reduces the surface tension of water−oil significantly. Surface tension will also vary with time. With the given range in surface tensions, the capillary number will be in the range 3×10^{-8} to 1.4×10^{-6}. Even for the largest capillary number, the tertiary fluid displacement will be dominated by the capillary forces.

Two series of experiments are performed: with and without SPAN80 surfactant added to the alkane. The fluid combinations are listed in Table 2. Additionally, four baseline experiments are conducted without salinity contrast, meaning that the resident water and invading water both have a salt concentration of 1.7 g/L. Each experiment is repeated twice to check the reproducibility. To observe the change of water and oil regions, a subdomain containing at least one LSW−oil-HSW cluster is continuously monitored for at least 70 h. The field-of-view is selected in such a way that we observe the full HSW domain, while both oil and LSW might have connections to volumes outside the field-of-view.

3. RESULTS AND DISCUSSION

3.1. Observation of HSW Expansion in Experiments without Surfactant. Given the large number of images, we mainly present results for experiment Nos. 1 and 4 in this section, while other results are shown in the Supporting Information. The observed domain has dimensions of 2,797.16 μm × 2,238.39 μm (width × height). For the 70 h of observation, we selected regions with initially stable LSW−oil−HSW systems, with the oil sandwiched between the disconnected HSW and the connected LSW. To analyze the images, we developed an image processing and data extraction method that is described in the Supporting Information. With our developed data extraction method, we obtained a quantitative analysis for the expansion rate of HSW areas, water volumetric flux, and the dimensionless flux in the oil phase.

3.1.1. Experiments with n-Heptane. We first consider the experiment No. 1 with pure *n*-heptane. Pictures of the observed domain at 0 and 70 h are shown in Figure 5. In this figure, blue areas represent 1.7 g/L LSW in the microchip. The oil phase is shown as the brown areas confined among LSW, grain, and HSW. The colorless regions along grains are the trapped 170 g/L HSW. We can easily filter out the area of the grains in an imaging process. We did not observe any emulsification during the whole monitoring period.

We notice that all HSW domains undergo significant swelling, and the curvature of the HSW−heptane interface gradually increases, resulting in the measurable displacement of heptane globules. We can see that both HSW−heptane and LSW−heptane interfaces moved as the distance between them decreasing slightly. This caused a change in the shape of heptane globules. This is clearly noticeable with HSW and oil phases found inside the purple dashed square. One interesting

Table 2. Types and Information of Microfluidic Experiments

| Experiment	Series	Oil type	Resident brine	Flooding brine	Remark
1	Without surfactant	n-heptane	HSW	LSW (1.7 g/L)	
2			HSW	LSW (50 g/L)	
3			LSW (1.7 g/L)	LSW (1.7 g/L)	baseline
4		n-dodecane	HSW	LSW (1.7 g/L)	
5			HSW	LSW (50 g/L)	
6			LSW (1.7 g/L)	LSW (1.7 g/L)	baseline
7	With surfactant	n-heptane + 1% SPAN 80	HSW	LSW (1.7 g/L)	
8			HSW	LSW (50 g/L)	
9			LSW (1.7 g/L)	LSW (1.7 g/L)	baseline
10		n-dodecane + 1% SPAN 80	HSW	LSW (1.7 g/L)	
11			HSW	LSW (50 g/L)	
12			LSW (1.7 g/L)	LSW (1.7 g/L)	baseline
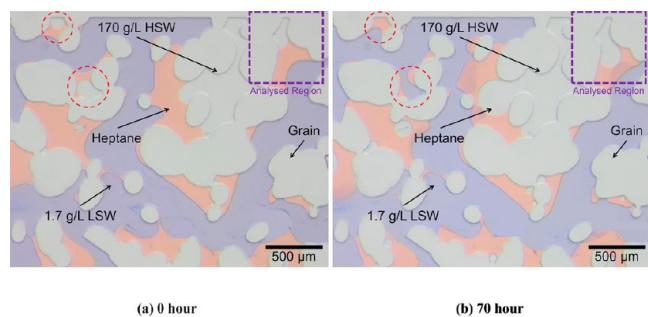
Figure 5. Images of fluid distributions in experiment No.1 observed at 0 and 70 h.

phenomenon is the sudden merge of HSW with LSW when the two phases touch each other; compare the red dashed circles in Figure 5, parts a and b. In this process, HSW joins the bulk LSW phase, and the oil phase is relocated and attached to the solid grains.

In the blue dashed areas, we observe that the distance among HSW and LSW interfaces gradually decreases within 70 h. Through measuring the HSW and oil areas, the HSW region grew by 119.4%, while the heptane area is nearly unchanged, shown in Figure 6a. Measurement error for all experiments is 3%. With the strong oil-wet microchip, we do not observe any thin water films of LSW along the grains. We consider that the increase in the HSW area is caused by water molecules penetrating the heptane region. The fluid pressure inside the HSW area increases due to the increased volume, which
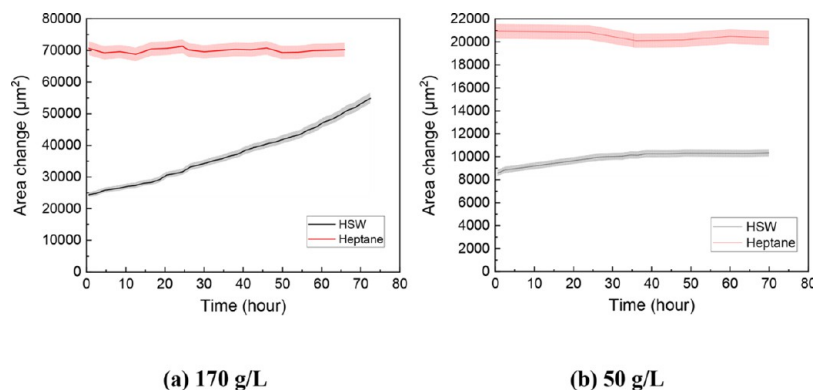
induces menisci deformation and displaces the oil out of the throat.

Images for the case of 50−170 g/L salinity contrast are shown in figure SI-1 of the Supporting Information. HSW area with lower salinity contrast has a slight growth by 20.7% until having a plateau after around 30 h (Figure 6b), while the oil region still keeps a constant area. In the baseline experiment No.3, we do not see any changes in brine and oil areas, indicating that there is no oil displacement and no water transport through oil under zero salinity gradient.

3.1.2. Experiments with n-Dodecane. Figure 7 gives the images of the observed domain of No. 4 experiment after 0 and

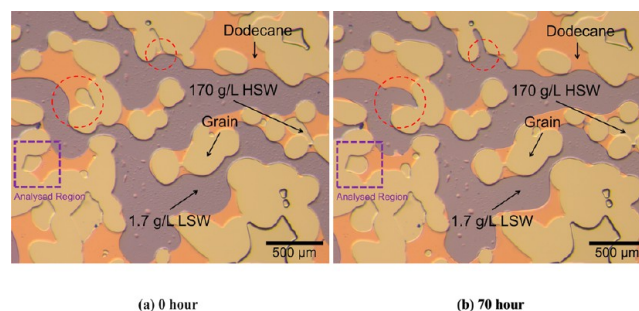**Figure 7.** Images of fluid distributions in experiment No. 4 observed after 0 and 70 h.

70 h. Similar to the experiment with heptane, all trapped HSW areas expands significantly. The phenomenon of HSW enclosure merging with LSW and the relocation of surrounding
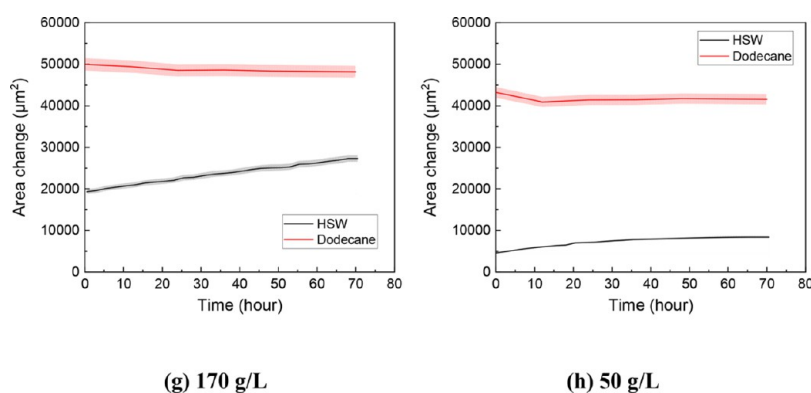

Figure 6. Measurements of heptane and HSW areas over 70 h for resident salinity concentrations of 170 and 50 g/L cases. Measurement error is shown in the shadow band.

(g) 170 g/L   **(h) 50 g/L**

Figure 8. Measurements of dodecane and HSW areas over 70 h for resident salinity concentrations of 170 and 50 g/L.

oil is also recorded. The region delineated by a blue dashed square is analyzed.

We observed that the HSW−dodecane interface is stretched and the distance among HSW and LSW interfaces gradually decreases. After measuring areas, see Figure 8, the HSW area grows by around 40% after 70 h of observation, while the oil area has minor changes. The HSW area continues to expand even after 70 h. For the case of 50 g/L HSW, the HSW area expands by 82.7% within the first 70 h. Curves of area change show a trend similar to that in experiments with heptane. After about 30 h, the HSW area does not change anymore, which means that water diffusion in the oil stops. Note that the amount of expansion cannot be compared for different areas and different experiments, because various regions have different initial areas of HSW, interface length of water−oil, and thickness of the oil the phase. However, in Section 4, we will display the dimensionless form for water flux to be able to compare different regions and experiments. The baseline experiment shows no obvious change in the trapped LSW areas.

3.2. Observation of Water Expansion when Oil Has Added Surfactant. To illustrate the surfactant effect on water transport, we performed eight experiments by adding 1% SPAN 80 to pure heptane and pure dodecane. The interfacial tension of water−decane has been reported to drop from 30 N/m to 10 N/m after about 1-h contact with water when the decane contains a concentration of 0.01 wt % SPAN80.[49] Besides, the presence of surfactant affects the emulsion stability, interface viscoelasticity and fluid coalescence.[50] Therefore, compared to the cases without a surfactant in the oil phase, emulsion formation around the water−oil interface is expected during the observation period. We also performed two baseline experiments with no salinity contrast for both surfactant-enhanced alkanes. In the following two subsections, only results of experiments Nos. 7 and 10 are presented. Other images and results can be found in the Supporting Information.

3.2.1. Experiments Using n-Heptane with SPAN80. Figure 9 presents the oil and water distributions in the observed domain for experiment No. 7 at 0, 3, 48, and 70 h after initialization. In the figures, the oil phase (orange) is heptane with 1% SPAN80 surfactant added, and the connected water (purple) is 1.7 g/L low-salinity brine. The region for analysis is marked with a blue dashed square. We capture the dynamic change of the shape of oil collars and coalescence between grains, as shown within the red dashed circles. At 3 h of observation, one oil collar is generated due to oil relocation surrounding two grains (see red circle in Figure 9b). The collar
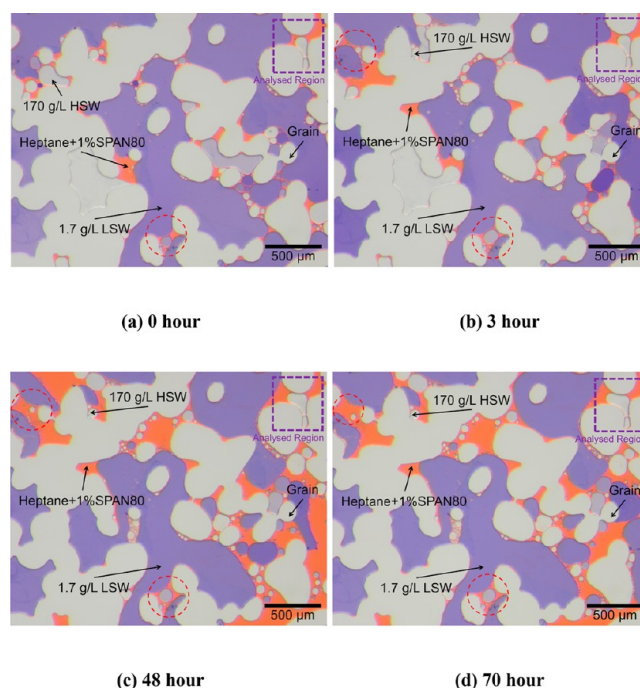

(a) 0 hour   **(b) 3 hour**

(c) 48 hour   **(d) 70 hour**

Figure 9. Images of the observed domain in experiment No. 7 at 0, 3, 48, and 70 h, where the oil phase is heptane with 1% SPAN80.

thickness gradually grows with the oil invasion and displacement from areas outside the observed domain. Another interesting phenomenon is that most HSW−oil droplets do not burst into LSW regions even when touching the LSW−oil interface. Instead, the HSW droplets are continuously swelling.

The varying emulsion and oil film thickness introduces difficulties in finding a stable system of LSW−oil−HSW for image and data analysis; however, the area indicated by the purple dashed square in Figure 9 captures an HSW region well. That region is shown in Figure 10a−f and observed changes are analyzed. The HSW area swells significantly and deforms at the throat. Unlike the experiment with pure heptane, the thin oil film along the grains contains multiple microemulsions and dynamically varies its film thickness with the accumulation and swelling of emulsions. Notably, within the monitoring period, next to the LSW−oil interface, many nano- to microscale emulsions are generated and the front of aggregated emulsions gradually invades into the oil phase, whereas no emulsions can be observed near the HSW−oil interface.
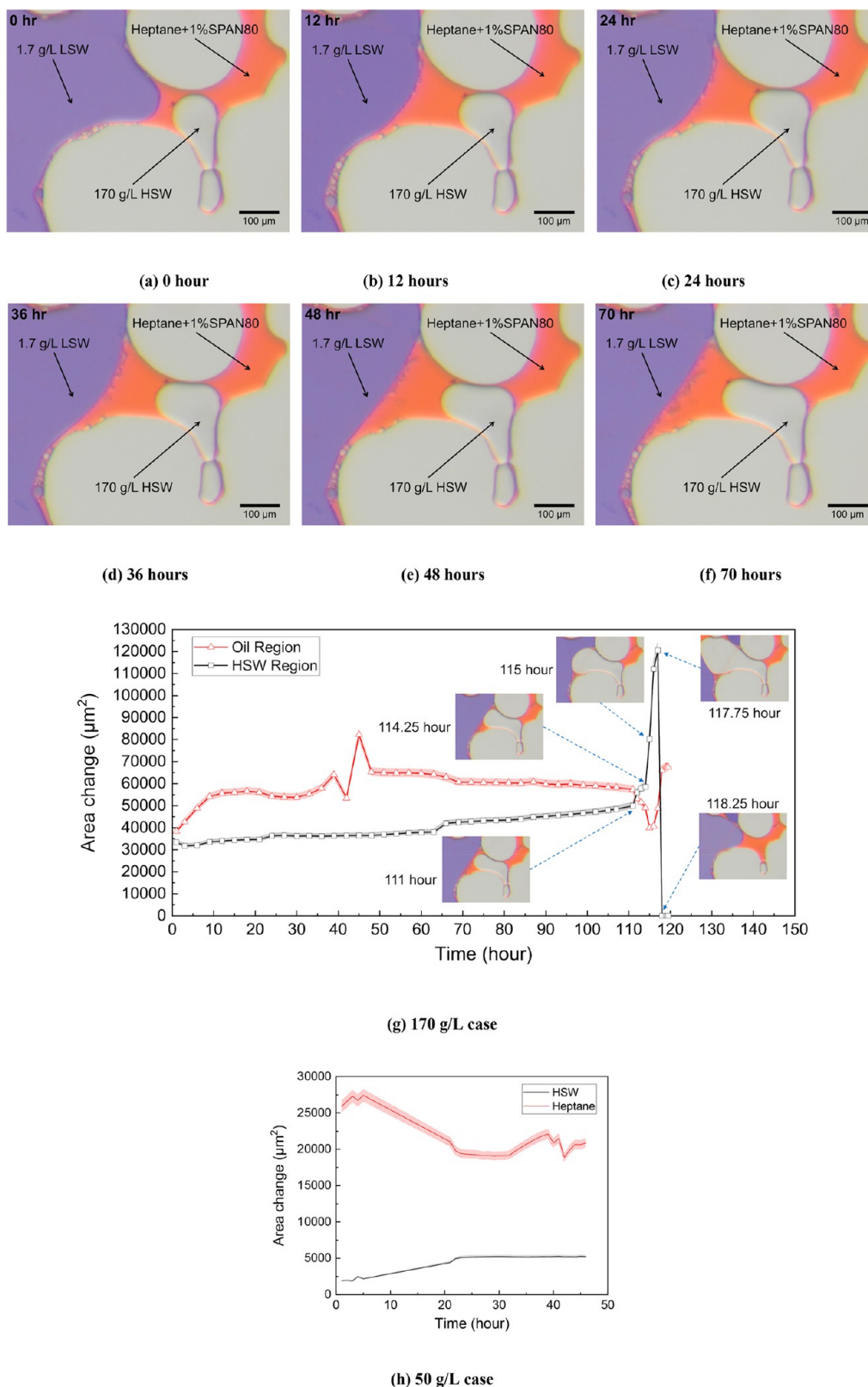
Figure 10. Pictures of an LSW-hepane + 1% SPAN80-HSW cluster from 0 to 70 h (a−f). 1.7 g/L LSW shows as purple and heptane shows as orange. (g) Changes in oil and HSW areas for 170 g/L case in 70 h. Five representative images for the sudden curve changes are added to point out the reason for these abrupt changes. (h) Results for the case with 50 g/L brine as resident water.

Figure 10g shows the oil and HSW area changes. The oil area shows unstable fluctuations, which is marked as the sudden jump between 40 and 50 h. Note that oil phase is connected to oil outside the area of observation; thus, the changes in the oil area are only indicative of movement of oil in and out of the domain and not of changes in oil volume due to

transfer between the phases. At 70 h, the analyzed HSW region has swelled by 28.24%, and it has a relatively stable increase before 111 h. The diagram also shows two stages of rapid growth in the HSW area when the HSW−oil interface is close to the LSW−oil interface. From 111 to 114.25 h of observation, the front of the HSW gradually expands out of the throat until almost touching the LS. Afterward, the HSW area dramatically expands and deforms within 3.5 h before merging with the LSW. This dramatic increase is induced by the short distance of transport when the two interfaces are separated by a thin oil film. Such a highly elastic oil film is not observed in the experiments with pure alkanes. Finally, the oil film cannot maintain its large deformation, and breaks, leading to a rapid mixing of the HSW and LSW. The images for the No.8 experiment with 50 g/L LSW are shown in the Supporting Information (Figures SI-8 and SI-9). From the measurements, the HSW area in the analyzed region has an expansion of 174.51% after 46 h. The plotted curve gives an obvious flat stage of HSW growth after around 23 h, similar to what was observed in experiment No. 4. The fluctuations in the oil area come from the unstable oil film along the solid surface. One notable phenomenon is that the generated oil films are much thinner (~2 μm thickness and 400 μm length between two grains in the 46 h image) than the ones in the experiments with pure n-heptane, displaying the high elasticity of oil−water interfaces with the help of surfactant. However, compared to the case of the 170 g/L case, there are no observed emulsions generated around LSW−oil and HSW−oil interfaces and no obvious expansion of trapped salinity water. This indicates that increased salinity (50 g/L in water) reduces the formation of microemulsion, which also means that a lower salinity contrast (50−170 g/L) inhibits water transport in oil phase.

3.2.2. Experiments with Dodecane with SPAN80. To study the impact of the carbon chain length of oil, we conducted experiments with surfactant-added n-dodecane (experiment No. 10). In Figure 11, we present images from this experiment at four different times. The analyzed region is marked with a blue dashed square. Most oil enclosures (or globules) are stable and displaced in and out of the observed domain through the film flow along the grain surfaces. Expansion in collar oil films is captured as well, shown in the left-hand red dashed circle. The red circles indicate the good malleability of the oil film due to the presence of SPAN80. The expanded HSW almost directly contacts the LSW−oil interface for 70 h but does not merge with the LSW because of the thin layer of oil between them. Unlike in experiment No.7 (heptane with surfactant), the n-dodecane does not contain multiple microemulsions and has less displacement in the observation period.

Enlarged images of the analyzed region are displayed in Figure 12. Within the first 70 h, the HSW area increases by 71.9% and gradually squeezes oil out of the pore space. Therefore, the thickness of the oil between the HSW−oil and LSW−oil interfaces decreases. The oil area continuously decreases because of the displacement. Around 74.5 h, the two interfaces are separated by a thin oil film only, and the HSW area suddenly increases by 89.77% in 2.5 h, as shown in Figure 12f. The HSW enclosure rapidly expanded into the throat. After 77 h, the HSW stops growing, and there appears to be an equilibrium between the HSW bubble and the surroundings. Another notable point is that fewer nano- to microemulsions are found around the LSW−oil interface
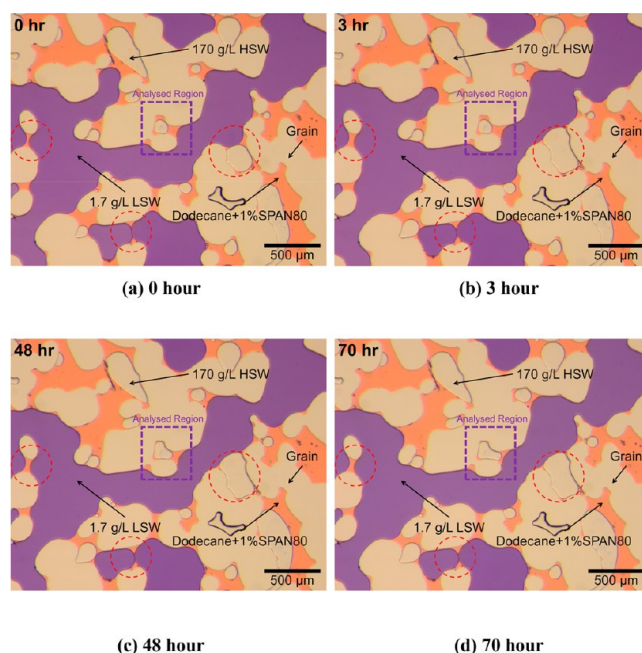

Figure 11. Images of the observed domain in experiment No. 7 at 0, 3, 48, and 70 h, where the oil phase is dodecane with 1% of SPAN80.

inside oil phases than in the experiments with heptane. The generated emulsions, e.g., the black dots and colorless water-in-oil emulsions, are almost stationary and have no significant swelling.

Experiment No. 11 with the salinity contrast of 50−170 g/L is shown in the Supporting Information. The measurements for oil and HSW areas are plotted in Figure 12h. The analyzed HSW area steadily swells by 26.4% in 48 h and reaches a plateau after around 34 h. The oil phase maintains a stable size after the sudden invasion of LSW due to the changing locations of the water−oil interfaces. In addition, a baseline case, experiment No. 12, with no salinity contrast, is also conducted for eliminating the influence of low ionic strength to the water−oil interface behavior. The images in the Supporting Information show no expansion of the disconnected water phase and no displacement of constrained oil, which indicates that the salinity contrast is essential for emulsification and oil mobilization in the systems of HSW−oil−LSW.

3.3. Pore−Scale Visualization of Spontaneous Emulsification. Spontaneous emulsification may occur when water and oil are in direct contact. The size of inverse micelles depends on brine salinity and surfactant concentration. Santana-Solano et al.[51] performed experiments to directly observe the spontaneous emulsification at the water−oil interface, and showed that inverse micelles swell with increased surfactant concentration. To capture the emulsification process, we increased the SPAN80 concentration in dodecane from 1% to 2%, while we used the high-salinity contrast of 1.7−170 g/L. Figure 13a−c shows the direct observation of the emulsions near an LSW−oil interface over the monitoring period. As high-salinity generally inhibits the formation of emulsification, only the LSW−oil interface has visible emulsions and dynamic aggregation. With the aggregation and growth of emulsions, the LSW−oil interface becomes coarse and the emulsion saturation zone expands. For other experiments with 1% SPAN 80 in the oil and 50−170 g/L brines, the emulsions either occurred as black dots or were too
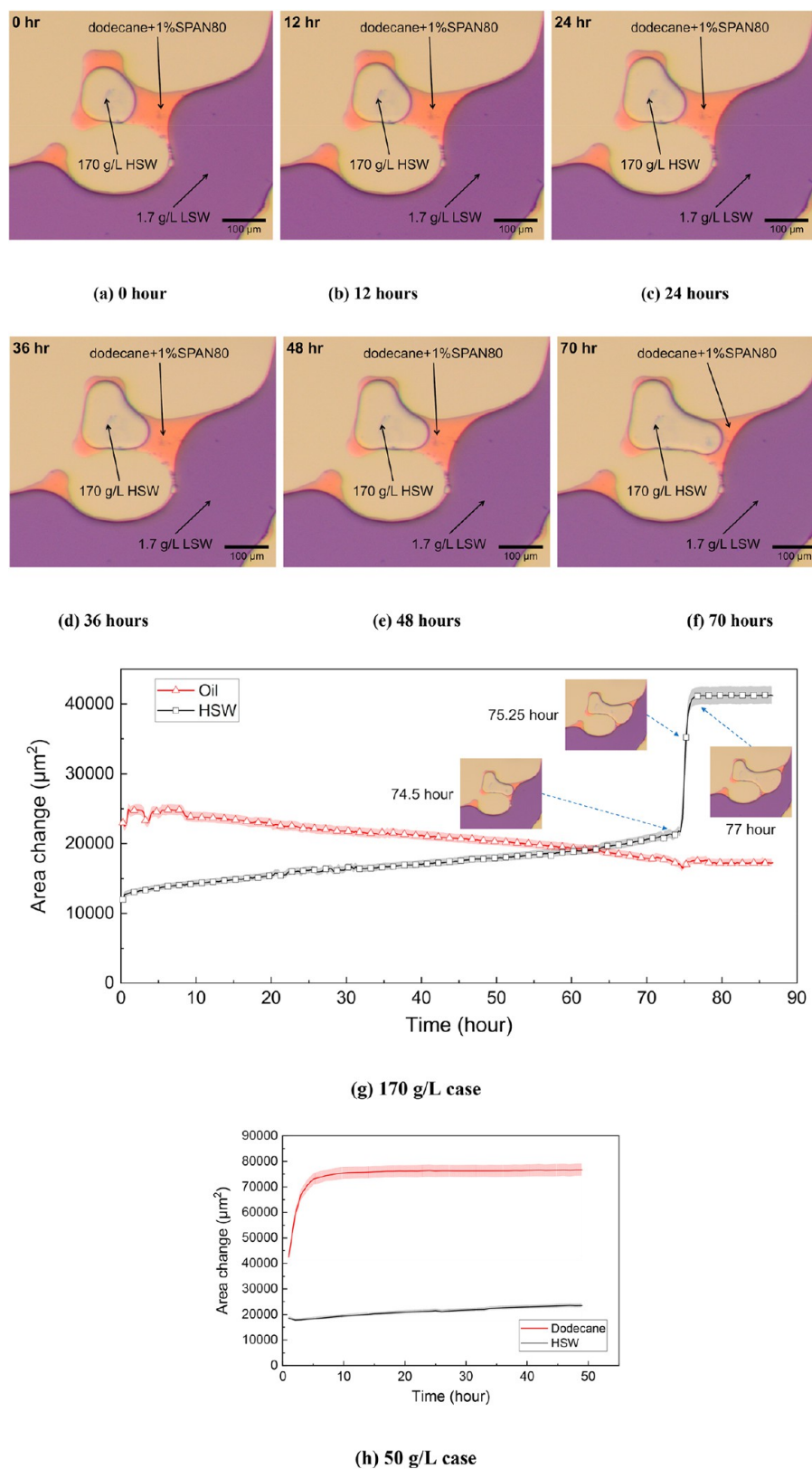
(a) 0 hour   (b) 12 hours   (c) 24 hours

(d) 36 hours   (e) 48 hours   (f) 70 hours

(g) 170 g/L case

(h) 50 g/L case

Figure 12. Images of the LSW-dodecane+1% SPAN80-HSW phases in the analyzed region at six moments within 70 h (a−f). (g) Changes of oil and HSW areas for this 1.7−170 g/L salinity contrast case during the 70 h. Three representative images for the sudden curve changes are added. (h) Results for the case with 50−170 g/L salinity contrast.

small to be captured by the camera. Using the literature value of 250 nm for the size of a single water-in-dodecane + SPAN80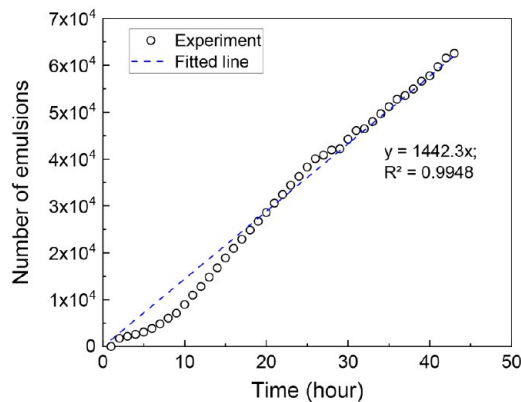 emulsion,[52] the number of emulsions can be estimated from the size of the saturation zone area, as shown in Figure 13d. The emulsion number displays a linear increase, and a linear fit is also plotted in the figure.
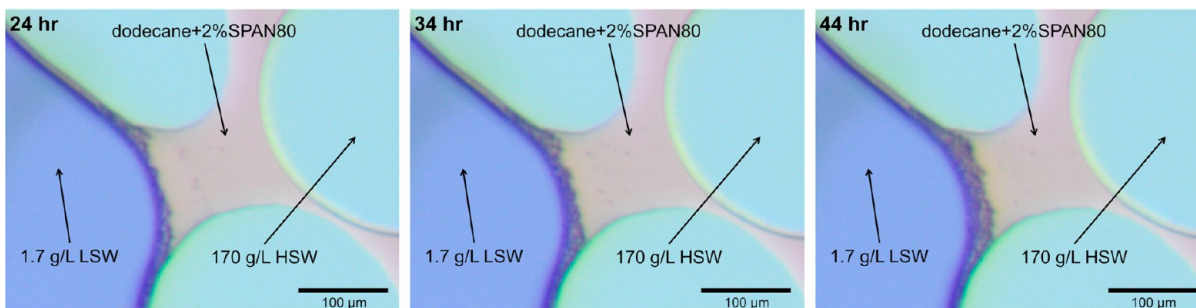
(a) 24 hours   **(b) 34 hours**   **(c) 43 hours**

(d) number of emulsions versus time

Figure 13. Images of spontaneous emulsification in the experiment using dodecane with 2% SPAN80. (a−c) Accumulation of water/oil emulsions at the LSW−oil interface after 24, 34, and 43 h. (d) A plot of the number of emulsions in the emulsion zone

3.4. Calculation of Water Flux in an Oil Phase. We approximate the water transport in the oil as a 1-D process with an averaged cross section, $A_{ave}^c = hL_{ave}$, where h thickness of the pore space (20 μm), and L_{ave} is the averaged length of the two water−oil interfaces. The water mass flux J_w in oil is calculated by Fick's law:

$$\int_{A_{ave}^c} J_w \, dA \simeq \overline{J}_w h L_{ave} = D_w \frac{c_{LSW} - c_{HSW}}{d_{oil}} h L_{ave} \qquad (1)$$

Here d_{oil} is the minimum thickness of oil, D_w is the water diffusion coefficient in oil, and c_{LSW} and c_{HSW} are the water concentrations in the oil at the LSW−oil interface and HSW−oil interface, respectively. The volume change rate of the HSW region, Q_w, can be described as follows:

$$Q_w = \frac{dV_{HSW}}{dt} = h\frac{dA_{HSW}}{dt} \qquad (2)$$

where A_{HSW} is a HSW area that can be obtained from images. Combining eq 1 and eq 2, we obtain the relationship:

$$D_w \frac{c_{LSW} - c_{HSW}}{d_{oil}} L_{ave} = \rho_w \frac{dA_{HSW}}{dt} \qquad (3)$$

Equation 3 gives us the water mass flux, $D_w(c_{LSW}-c_{HSW})/d_{oil}$, in oil phase with different salinity conditions. From the literature,[53] the water diffusion coefficients in two types of oil are around 7.4×10^{-9} m²/s and 3.0×10^{-9} m²/s,

respectively. A typical size of water−SPAN80−oil reverse micelle is 5 nm.[54] The diffusion coefficient of one single micelle in oil phase can be calculated by using the Stokes−Einstein equation

$$D = \frac{k_B T}{6\pi\eta r} \qquad (4)$$

where η is the dynamic viscosity, k_B is Boltzmann's constant, T is the absolute temperature, and r is the radius of the reverse micelle. Therefore, the diffusion coefficients of one reverse micelle for heptane and dodecane are 1.2×10^{-10} m²/s and 3.2×10^{-11} m²/s. With the difficulty of providing an exact relationship between ionic strength and water concentration in the oil phase, we only estimated the concentration difference at the LSW−oil interface and HSW−oil interface ($c_{LSW} - c_{HSW}$) based on the above equations.

In order to evaluate water volumetric flux in oil for various experiment, baseline parameters are introduced as $t_{ref} = \frac{d_{oil}A_0}{D_w L_{ave}}$, and $Q_{ref} = \frac{hA_0}{t_{ref}}$, where A_0 is the initial area of HSW. Therefore, all parameters in dimensionless forms become, $A^* = A_{HSW}/A_0$, $t^* = t/t_{ref}$, and $Q^* = \frac{Q_w}{Q_{ref}} = \frac{d_{oil}}{D_w L_{ave}}\frac{dA_{HSW}}{dt}$.

3.5. Effects of Salinity, Carbon Length, and SPAN80 on the Water Transport in Oil. Figure 14 presents the plots of dimensionless water volumetric flux versus dimensionless
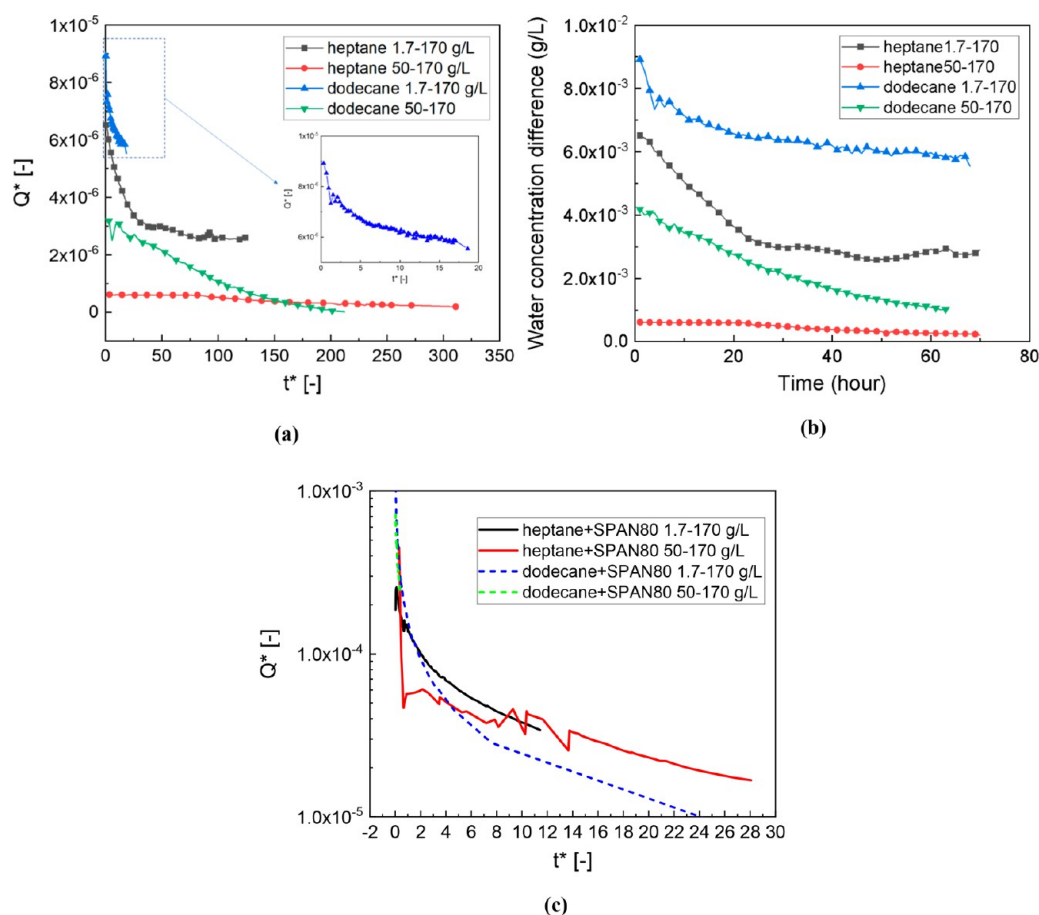
Figure 14. Relationships between dimensionless water volumetric flux and time. (a) Comparison between the absence and presence of SPAN80 in two pure alkanes. (b) Effect of SPAN80 on the water fluxes. (c) Change in concentration difference of water between the two brine−oil interfaces.

Table 3. Comparison of Dimensionless Water Flux and Concentration Difference for Various Experiments

Exp. No	Series	Alkane type	Salinity contrast (LSW−HSW)	Dimensionless water flux ($\times 10^{-6}$ [−])	Water concentration difference ($\times 10^{-3}$ g/L)
1.	Without SPAN80	*n*-heptane	1.7−170	3.13	3.47
2			50−170	0.40	0.43
3		*n*-dodecane	1.7−170	6.43	6.45
4			50−170	1.19	2.23
5	With SPAN80	*n*-heptane + SPAN 80	1.7−170	70.66	162.68
6			50−170	34.70	378.54
7		*n*-dodecane + SPAN 80	1.7−170	101.20	507.61
8			50−170	395.75	427.53

time (Q^* vs t^*) for the absence and presence of SPAN80 in alkanes. To compare the water flux, we calculate and list the dimensionless water fluxes and water concentrations over the two water−oil interfaces for various experiments in Table 3. Within pure heptane, the average values of dimensionless water flux are 3.13×10^{-6} and 4.02×10^{-7} for the salinity contrasts of 1.7−170 g/L and 50−170 g/L, respectively, while the corresponding values for dodecane are 6.43×10^{-6} and 1.19×10^{-6}. We see that in both cases of pure heptane and pure dodecane, Figure 14a, a higher salinity contrast contributes to a larger water flux. The water fluxes have a nonlinear change over time, with a significant drop for $t^* < 100$, after which the flux gradually flattens and becomes stable, especially for the cases with 50−170 salinity contrast reaching zero water flux around $t^* > 200$. Moreover, the results show that dodecane, with the longer carbon length, yields a larger water flux than heptane for

both salinity contrasts. Correspondingly, the water concentration difference ($c_{LSW} - c_{HSW}$, mentioned above) between the HSW−oil interface and the LSW−oil interface has a similar trend as the water flux during the experimental period, as seen in Figure 14b. The concentration difference change proves that salinity plays a critical role in the water solubility and diffusion in oil. With the presence of SPAN80, shown in Figure 14c, the four volumetric water fluxes are almost 100 times higher and have even higher initial values than those in pure alkanes phases. Early in the experiments, for $0 < t^* < 4$, the fluxes decrease dramatically before reaching relatively stable states. The average values of water concentration difference for the SPAN80-added experiments are about 47 to 876 times larger than those for pure alkane experiments. Interestingly, the curves do not display a clear distinction between heptane and dodecane, and no clear distinction between the two salinity
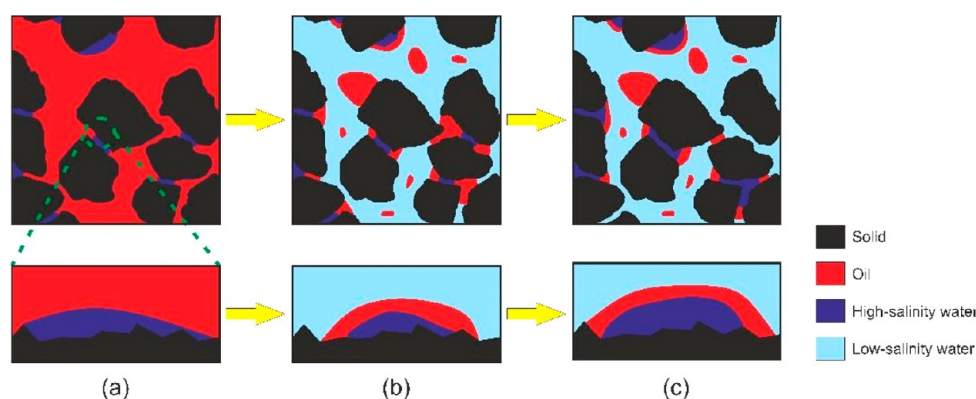
Figure 15. 2D Schematics of changes in brine-oil-solid contact during a low-salinity water displacement. (a) Initial state of connate water and crude oil in a porous domain, (b) state after low-salinity water flooding, and (c) state after a long-term contact among LSW, oil, and HSW.
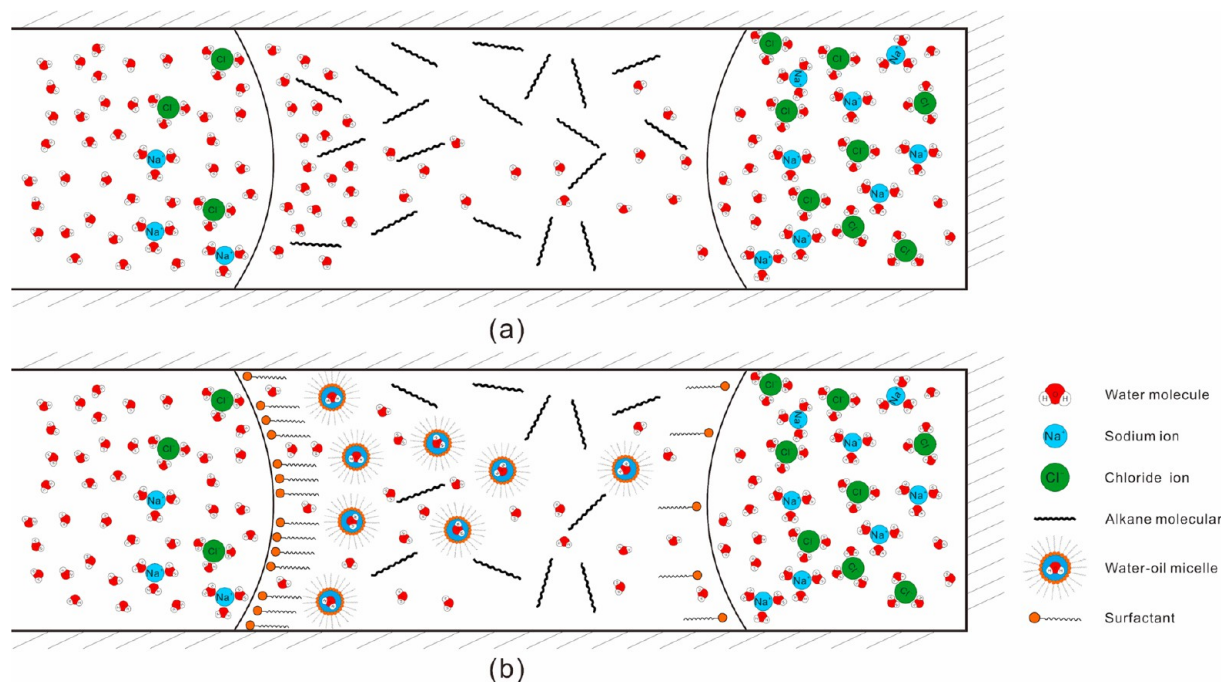

Figure 16. Schematics of water transport through the oil phase under salinity difference: (a) one scenario for water diffusion induced by chemical potential; (b) another scenario for water transport induced by chemical potential and micelle transport.

contrasts. This indicates that SPAN80 plays a dominant role in the water transport, and eliminates the effect of carbon length to some extent.

4. HYPOTHESIS ON WATER TRANSPORT IN AN OIL PHASE

During the low-salinity water flooding, the three-phase contact line of water−oil-solid undergoes significant changes, as shown in Figure 15 and described below. Before water injection into the micromodel, connate water (high-salinity brine) and crude oil fill the pore space. With the injection of low-salinity water, most of the crude oil is displaced, with connate water still being trapped by the crude oil. The trapped connate water gradually grows through the two scenarios described in the Introduction: water diffusion through oil and water transport through a brine film. Consequently, the oil droplet moves due to water expansion. Due to the oil-wet solid surface after wettability modification, the second scenario has less

possibility to occur. Therefore, the water molecule has a higher chance to penetrate the oil phase.

We propose two processes of water transport through oil to explain the observations in the pore-scale experiments: water diffusion for pure alkanes and water transport via the movement of reversed micelles when surfactants are present. These two processes are illustrated in Figure 16. In the first scenario, for alkanes without surfactants (Figure 16a), the HSW−oil interface and LSW−oil interface contain different water concentrations inside the oil, resulting from the salinity effect on water solubility. Schatzberg[55] and Heidman et al.[56] both proposed that high-salinity has the potential to cause a lower water solubility in oil, while low-salinity causes a higher value of water concentration in oil. The interface of LSW−oil therefore contains more water than that of HSW−oil. Due to the chemical potential, water molecules diffuse from the LSW−oil interface toward the HSW−oil side. This hypothesis has been supported by molecular dynamic simulations to describe the trajectory of water molecules movements inside heptane

phases.[40] In the second scenario (Figure 16b), the surfactant molecules gather on the water−oil interface to minimize the free energy. The concentration of surfactant molecules at water−oil interfaces depends on the salinity concentrations.[57] When the concentration of surfactants is higher than the critical micelles concentration (CMC), micelles or reverse micelles (depending on the type of surfactant, either oil-soluble or water-soluble, respectively) will be generated by diffused water molecules and dissociative polar components and eventually form microemulsion droplets dispersed in the oil. In this work, we discuss only the case of reverse micelles, meaning that water is in the core of reverse micelles. Although the emulsion concentration increases, the nucleated emulsion droplets still keep as a group and coalesce into larger emulsions due to Gibbs free energy and entropic limitations.[58] Accordingly, the high-salinity water interface has no emulsification. The increase of ionic strength has a potential to lead more asphaltene and resin molecules to accumulate around the oil−water interface, resulting in more compact and rigid films.[59]

The repulsion between the charges of micelles induces micelle movement, which gradually pushes them away from the water−oil interface. Reverse micelles are capable of significantly contributing to water transport through organic liquids.[60,61] Wen and Papadopoulos[62] directly observed the process of microemulsion repulsion and water transport in water/oil/water emulsions during spontaneous emulsification. They also proved that the water transport rate in organic phases via reverse micelles is independent of the salt difference between the two sides of the organic phases. Similarly, in our hypothesis, the repelled emulsions help water transport from the LSW−oil interface to the HSW−oil interface, which changes the interfacial elasticity and enhances the speed of HSW region expansion. The salt concentration influences the concentration of spontaneously formed reverse micelles. Higher ionic strength gives lower concentration and slows down the swelling of the reverse micelle.[61] Additionally, the water transport in oil could be accelerated under reservoir temperature conditions due to the molecules' faster movement. The kinetic behavior of water molecules in oil will be further discussed in future studies.

5. SUMMARY AND CONCLUSIONS

We have conducted 12 sets of microfluidic experiments to research the salinity effect and the role of surfactant in the oil. The results with pure alkanes indicate that the HSW volume (estimated from the area in planar images) has a gradual increase, while the surrounding oil approximately retains its original size. Because the solid surface is oil-wet, water films along the grain surfaces were not observed; therefore, the swelling of the HSW was assumed to be induced by water transport through oil. Furthermore, the experiments with the addition of 1 wt % SPAN80 to the alkanes were able to illustrate the contribution of emulsification on water transport through oil. To capture the process of spontaneous emulsification, we conducted an additional experiment by adding 2 wt % SPAN80 surfactant in dodecane and observed and quantified the dynamic process of emulsion generation and saturation zone growth. The main conclusions are pointed out as follows:

- A hypothesis for explaining water transport through the oil phase is proposed: water diffusion and micro-emulsions transport in the oil phases.

- The direct pore-scale evidence of water transport in oil under different salinity contrasts is provided, where the effect of salinity contrast on the trapped HSW expansion is directly observed. The constrained oil between LSW and HSW is accordingly redistributed in the pore space.

- A higher salinity contrast of 1.7−170 g/L induces a faster water flux in both of heptane and dodecane than the contrast of 50−170 g/L.

- Adding SPAN80 to alkanes enhances the water flux more than 100 times, thereby overshadowing salinity effect on water flux in oil. The introduction of surfactant increases the elasticity of the water−oil interface, which is reflected by significant deformation of swelling HSW bubbles before rupture.

- The difference of water concentration is evaluated between LSW−oil and HSW−oil interfaces. In the presence of surfactant, the water concentration difference is found to be at least 47 times larger than in pure alkanes.

- The dynamic processes of emulsion generation and a growing saturation emulsion zone are captured in an experiment with dodecane and 2 wt % SPAN80.

■ ASSOCIATED CONTENT

ⓈⒾ Supporting Information

The Supporting Information is available free of charge at https://pubs.acs.org/doi/10.1021/acs.energyfuels.3c02245.

Results and data of experiments 2, 3, 5, 6, 8, 9, 11, and 12 (PDF)

■ AUTHOR INFORMATION

Corresponding Authors

Lifei Yan − *Environmental Hydrogeology, Department of Earth Sciences, Utrecht University, 3584 CB Utrecht, The Netherlands; Faculty of Civil Engineering and Geosciences, Delft University of Technology, 2600 GA Delft, The Netherlands;* ⓞ orcid.org/0000-0001-8774-3357; Email: l.yan@uu.nl

Amir Raoof − *Environmental Hydrogeology, Department of Earth Sciences, Utrecht University, 3584 CB Utrecht, The Netherlands;* Email: A.Raoof@uu.nl

Authors

Mohammad Hossein Golestan − *PoreLab, Department of Geoscience and Petroleum, NTNU, 7031 Trondheim, Norway*

Wenyu Zhou − *PoreLab, Department of Geoscience and Petroleum, NTNU, 7031 Trondheim, Norway*

S. Majid Hassanizadeh − *Environmental Hydrogeology, Department of Earth Sciences, Utrecht University, 3584 CB Utrecht, The Netherlands; Center of Excellence for Simulation Technology (SimTech), Stuttgart University, 70049 Stuttgart, Germany*

Carl Fredrik Berg − *PoreLab, Department of Geoscience and Petroleum, NTNU, 7031 Trondheim, Norway*

Complete contact information is available at:
https://pubs.acs.org/10.1021/acs.energyfuels.3c02245

Notes

The authors declare no competing financial interest.

■ NOMENCLATURE

LSW=low-salinity water
HSW=high-salinity water
LS=low-salinity
MIE=multiple ion exchange
DLVO=Derjaguin, Landau, Verwey, and Overbeek
SEM=scanning electron microscopy
vdW=van der Waals forces
EDL=structural forces and electrostatic double layer
CMC=critical micelle concentration
W/O=water in oil
O/W=oil in water

■ REFERENCES

(1) Tang, G.; Morrow, N. R. Salinity, temperature, oil composition, and oil recovery by waterflooding. *SPE Reservoir Engineering* **1997**, *12* (04), 269−276.

(2) Buckley, J.; Liu, Y.; Monsterleet, S. Mechanisms of wetting alteration by crude oils. *SPE journal* **1998**, *3* (01), 54−61.

(3) Lager, A.; Webb, K. J.; Black, C.; Singleton, M.; Sorbie, K. S. Low salinity oil recovery-an experimental investigation1. *Petrophysics* **2008**, *49* (01), 28−35.

(4) Ligthelm, D. J.; Gronsveld, J.; Hofman, J.; Brussee, N.; Marcelis, F.; van der Linde, H. . Novel Waterflooding Strategy By Manipulation Of Injection Brine CompositionIn *EUROPEC/EAGE Conference and Exhibition*; Society of Petroleum Engineers: 2009; p SPE-119835-MS; .

(5) Zhang, Y.; Morrow, N. R. Comparison of secondary and tertiary recovery with change in injection brine composition for crude-oil/sandstone combinations. In *SPE/DOE Symposium on Improved Oil Recovery*; Society of Petroleum Engineers: 2006; p SPE-99757-MS; .

(6) McGuire, P.; Chatham, J.; Paskvan, F.; Sommer, D.; Carini, F. Low salinity oil recovery: An exciting new EOR opportunity for Alaska's North Slope. In *SPE Western Regional Meeting*; Society of Petroleum Engineers: 2005; p SPE-93903-MS; .

(7) Emadi, A.; Sohrabi, M. Visual investigation of oil recovery by low salinity water injection: formation of water micro-dispersions and wettability alteration. In *Proc. SPE Ann. Tech. Conf. Exhib.*; Society of Petroleum Engineers: 2013; Vol. *6*, p 166435-MS; .

(8) Sandengen, K.; Arntzen, O. Osmosis during low salinity water flooding. In *IOR 2013−17th European Symposium on Improved Oil Recovery*; European Association of Geoscientists & Engineers: **2013**; p cp-342-00015; .

(9) Tang, G.-Q.; Morrow, N. R. Influence of brine composition and fines migration on crude oil/brine/rock interactions and oil recovery. *J. Pet. Sci. Eng.* **1999**, *24* (2−4), 99−111.

(10) Alhuraishawy, A. K.; Bai, B.; Wei, M.; Geng, J.; Pu, J. Mineral dissolution and fine migration effect on oil recovery factor by low-salinity water flooding in low-permeability sandstone reservoir. *Fuel* **2018**, *220*, 898−907.

(11) Jadhunandan, P.; Morrow, N. R. Effect of wettability on waterflood recovery for crude-oil/brine/rock systems. *SPE reservoir engineering* **1995**, *10* (01), 40−46.

(12) Sharma, M.; Filoco, P. Effect of brine salinity and crude-oil properties on oil recovery and residual saturations. *Spe Journal* **2000**, *5* (03), 293−300.

(13) Vledder, P.; Fonseca, J. C.; Wells, T.; Gonzalez, I.; Ligthelm, D. Low salinity water flooding: proof of wettability alteration on a field wide scale. In *SPE Improved Oil Recovery Symposium*; OnePetro: 2010; pp SPE-129564-MS.SPE-129564-MS.

(14) Tetteh, J. T.; Brady, P. V.; Barati Ghahfarokhi, R. Review of low salinity waterflooding in carbonate rocks: mechanisms, investigation techniques, and future directions. *Adv. Colloid Interface Sci.* **2020**, *284*, No. 102253.

(15) Ding, H.; Rahman, S. Experimental and theoretical study of wettability alteration during low salinity water flooding-an state of the art review. *Colloids Surf., A* **2017**, *520*, 622−639.

(16) Alshakhs, M. J.; Kovscek, A. R. Understanding the role of brine ionic composition on oil recovery by assessment of wettability from colloidal forces. *Advances in colloid and interface science* **2016**, *233*, 126−138.

(17) Mahani, H.; Keya, A. L.; Berg, S.; Bartels, W.-B.; Nasralla, R.; Rossen, W. R. Insights into the mechanism of wettability alteration by low-salinity flooding (LSF) in carbonates. *Energy Fuels* **2015**, *29* (3), 1352−1367.

(18) Aseyednezhad, S.; Yan, L.; Hassanizadeh, S. M.; Raoof, A. An accurate reduced-dimension numerical model for evolution of electrical potential and ionic concentration distributions in a nano-scale thin aqueous film. *Advances in Water Resources* **2022**, *159*, No. 104058.

(19) Strand, S.; Høgnesen, E. J.; Austad, T. Wettability alteration of carbonates—Effects of potential determining ions (Ca2+ and SO42−) and temperature. *Colloids Surf., A* **2006**, *275* (1−3), 1−10.

(20) Zhang, P.; Tweheyo, M. T.; Austad, T. Wettability alteration and improved oil recovery by spontaneous imbibition of seawater into chalk: Impact of the potential determining ions Ca2+, Mg2+, and SO42−. *Colloids Surf., A* **2007**, *301* (1−3), 199−208.

(21) Fathi, S. J.; Austad, T.; Strand, S. Smart water" as a wettability modifier in chalk: the effect of salinity and ionic composition. *Energy Fuels* **2010**, *24* (4), 2514−2519.

(22) Karimi, M.; Al-Maamari, R. S.; Ayatollahi, S.; Mehranbod, N. Impact of sulfate ions on wettability alteration of oil-wet calcite in the absence and presence of cationic surfactant. *Energy Fuels* **2016**, *30* (2), 819−829.

(23) Tetteh, J. T.; Veisi, M.; Brady, P. V.; Barati Ghahfarokhi, R. Surface reactivity analysis of the crude oil−brine−limestone interface for a comprehensive understanding of the low-salinity waterflooding mechanism. *Energy Fuels* **2020**, *34* (3), 2739−2756.

(24) Austad, T., Water-based EOR in carbonates and sandstones: new chemical understanding of the EOR potential using "smart water". In *Enhanced oil recovery Field case studies*; Elsevier: 2013; pp 301−335.

(25) Zhang, Y.; Xie, X.; Morrow, N. R. Waterflood performance by injection of brine with different salinity for reservoir cores. In *SPE Annual Technical Conference and Exhibition*; OnePetro: 2007; p SPE-109849-MS.

(26) Garcia-Olvera, G.; Alvarado, V. Interfacial rheological insights of sulfate-enriched smart-water at low and high-salinity in carbonates. *Fuel* **2017**, *207*, 402−412.

(27) Mokhtari, R.; Ayatollahi, S.; Fatemi, M. Experimental investigation of the influence of fluid-fluid interactions on oil recovery during low salinity water flooding. *J. Pet. Sci. Eng.* **2019**, *182*, No. 106194.

(28) Sheng, J. J. Critical review of low-salinity waterflooding. *J. Pet. Sci. Eng.* **2014**, *120*, 216−224.

(29) Hong, J.; Wang, Z.; Li, J.; Xu, Y.; Xin, H. Effect of Interface Structure and Behavior on the Fluid Flow Characteristics and Phase Interaction in the Petroleum Industry: State of the Art Review and Outlook. *Energy Fuels* **2023**, *37*, 9914−9937.

(30) Vaidya, R.; Fogler, H. Fines migration and formation damage: influence of pH and ion exchange. *SPE production engineering* 1992, 7 (04), 325−330.

(31) Sheng, J. *Modern chemical enhanced oil recovery: theory and practice*; Gulf Professional Publishing: 2010.

(32) Mahzari, P.; Sohrabi, M. Crude oil/brine interactions and spontaneous formation of micro-dispersions in low salinity water injection. In *SPE Improved Oil Recovery Symposium*; Society of Petroleum Engineers: 2014; pSPE-169081-MS; .

(33) Young, A.; Low, P. F. Osmosis in argillaceous rocks. *AAPG Bulletin* 1965, 49 (7), 1004−1007.

(34) Marine, I. W.; Fritz, S. J. Osmotic model to explain anomalous hydraulic heads. *Water Resour. Res.* 1981, 17 (1), 73−82.

(35) Neuzil, C. Osmotic generation of 'anomalous' fluid pressures in geological environments. *Nature* 2000, 403 (6766), 182−184.

(36) Fakcharoenphol, P.; Kurtoglu, B.; Kazemi, H.; Charoenwongsa, S.; Wu, Y.-S. The effect of osmotic pressure on improve oil recovery from fractured shale formations. In *SPE Unconventional Resources Conference*; OnePetro: 2014; p SPE-168998-MS; .

(37) Schmid, K.; Gross, J.; Helmig, R. Chemical osmosis in two-phase flow and salinity-dependent capillary pressures in rocks with microporosity. *Water Resour. Res.* 2014, 50 (2), 763−789.

(38) Sandengen, K.; Kristoffersen, A.; Melhuus, K.; Jøsang, L. O. Osmosis as mechanism for low-salinity enhanced oil recovery. *Spe Journal* 2016, 21 (04), 1227−1235.

(39) Yan, L.; Aslannejad, H.; Hassanizadeh, S. M.; Raoof, A. Impact of water salinity differential on a crude oil droplet constrained in a capillary: Pore-scale mechanisms. *Fuel* 2020, 274, No. 117798.

(40) Yan, L.; Chang, Y.; Hassanizadeh, S. M.; Xiao, S.; Raoof, A.; Berg, C. F.; He, J. A quantitative study of salinity effect on water diffusion in n-alkane phases: From pore-scale experiments to molecular dynamic simulation. *Fuel* 2022, 324, No. 124716.

(41) López-Montilla, J. C.; Herrera-Morales, P. E.; Pandey, S.; Shah, D. O. Spontaneous emulsification: mechanisms, physicochemical aspects, modeling, and applications. *J. Dispersion Sci. Technol.* 2002, 23 (1−3), 219−268.

(42) Li, Z.; Xu, D.; Yuan, Y.; Wu, H.; Hou, J.; Kang, W.; Bai, B. Advances of spontaneous emulsification and its important applications in enhanced oil recovery process. *Advances in colloid and interface science* 2020, 277, No. 102119.

(43) Martínez-Palou, R.; Cerón-Camacho, R.; Chávez, B.; Vallejo, A. A.; Villanueva-Negrete, D.; Castellanos, J.; Karamath, J.; Reyes, J.; Aburto, J. Demulsification of heavy crude oil-in-water emulsions: A comparative study between microwave and thermal heating. *Fuel* 2013, 113, 407−414.

(44) Rodríguez-Hakim, M.; Anand, S.; Tajuelo, J.; Yao, Z.; Kannan, A.; Fuller, G. G. Asphaltene-induced spontaneous emulsification: Effects of interfacial co-adsorption and viscoelasticity. *J. Rheol.* 2020, 64 (4), 799−816.

(45) Wu, T.; Firoozabadi, A. Surfactant-Enhanced Spontaneous Emulsification Near the Crude Oil−Water Interface. *Langmuir* 2021, 37 (15), 4736−4743.

(46) Du, Y.; Xu, K.; Mejia, L.; Zhu, P.; Balhoff, M. T. Microfluidic investigation of low-salinity effects during oil recovery: a no-clay and time-dependent mechanism. *Spe Journal* 2019, 24 (06), 2841−2858.

(47) Salehpour, M.; Sakhaei, Z.; Salehinezhad, R.; Mahani, H.; Riazi, M. Contribution of water-in-oil emulsion formation and pressure fluctuations to low salinity waterflooding of asphaltic oils: A pore-scale perspective. *J. Pet. Sci. Eng.* 2021, 203, No. 108597.

(48) Maaref, S.; Ayatollahi, S. The effect of brine salinity on water-in-oil emulsion stability through droplet size distribution analysis: A case study. *J. Dispersion Sci. Technol.* 2018, 39 (5), 721−733.

(49) Behera, M. R.; Varade, S. R.; Ghosh, P.; Paul, P.; Negi, A. S. Foaming in micellar solutions: Effects of surfactant, salt, and oil concentrations. *Ind. Eng. Chem. Res.* 2014, 53 (48), 18497−18507.

(50) Zabar, M. K.; Nguyen, C. V.; Phan, C. M. Quantifying the influence of salinity on spontaneous emulsification of hydrocarbons. *Colloids Surf., A* 2020, 588, No. 124376.

(51) Santana-Solano, J.; Quezada, C. M.; Ozuna-Chacón, S.; Arauz-Lara, J. L. Spontaneous emulsification at the water/oil interface. *Colloids Surf., A* 2012, 399, 78−82.

(52) Guha, I. F.; Anand, S.; Varanasi, K. K. Creating nanoscale emulsions using condensation. *Nat. Commun.* 2017, 8 (1), 1−7.

(53) Su, J. T.; Duncan, P. B.; Momaya, A.; Jutila, A.; Needham, D. The effect of hydrogen bonding on the diffusion of water in n-alkanes and n-alcohols measured with a novel single microdroplet method. *J. Chem. Phys.* 2010, 132 (4), No. 044506.

(54) Kopanichuk, I. V.; Vedenchuk, E. A.; Koneva, A. S.; Vanin, A. A. Structural properties of Span 80/Tween 80 reverse micelles by molecular dynamics simulations. *J. Phys. Chem. B* 2018, 122 (33), 8047−8055.

(55) Schatzberg, P. Solubilities of water in several normal alkanes from C7 to C161. *J. Phys. Chem.* 1963, 67 (4), 776−779.

(56) Heidman, J.; Tsonopoulos, C.; Brady, C.; Wilson, G. High-temperature mutual solubilities of hydrocarbons and water. Part II: Ethylbenzene, ethylcyclohexane, and n-octane. *AIChE journal* 1985, 31 (3), 376−384.

(57) Belhaj, A. F.; Elraies, K. A.; Mahmood, S. M.; Zulkifli, N. N.; Akbari, S.; Hussien, O. S. The effect of surfactant concentration, salinity, temperature, and pH on surfactant adsorption for chemical enhanced oil recovery: a review. *Journal of Petroleum Exploration and Production Technology* 2020, 10, 125−137.

(58) Miller, C. A. Spontaneous emulsification produced by diffusion—a review. *Colloids Surf.* 1988, 29 (1), 89−102.

(59) Binks, B. P.; Clint, J. H. Solid wettability from surface energy components: relevance to Pickering emulsions. *Langmuir* 2002, 18 (4), 1270−1273.

(60) Aldousary, S.; Kovscek, A. R. The diffusion of water through oil contributes to spontaneous emulsification during low salinity waterflooding. *J. Pet. Sci. Eng.* 2019, 179, 606−614.

(61) Mokhtari, R.; Ayatollahi, S. Dissociation of polar oil components in low salinity water and its impact on crude oil−brine interfacial interactions and physical properties. *Petroleum Science* 2019, 16 (2), 328−343.

(62) Wen, L.; Papadopoulos, K. D. Visualization of water transport in W1/O/W2 emulsions. *Colloids and surfaces A: Physicochemical and engineering aspects* 2000, 174 (1−2), 159−167.